社團法人中華鋪面工程學會
Chinese Society of Pavement Engineering

ORIGINAL RESEARCH PAPER

Bearing Capacity Characteristics of Compacted Cement Stabilized Gravel Pile Composite Foundation

Fei Gao[1] · Xuansheng Cheng[1] · Yanxu Zhao[2] · Qingfeng Lv[3] · Xiangjun Chen[2]

Abstract
Compacted cement stabilized gravel pile can effectively control secondary disasters of subgrade, while the bearing mechanism of semi-rigid pile composite foundation is not clear. The load–settlement (Q–S) curves, pile mechanical features and pile–soil stress characteristics of the composite foundation were analyzed by field tests and numerical simulation. Moreover, the characteristic value and calculating equation of the bearing capacity were discussed. Results show that the axial force of the group pile in composite foundation increases first and then decreases with the depth, the negative friction resistance is in the upper part, the neutral point is located at one-fifth of the length below the top. The lateral friction of the lower part of the pile plays a role before the upper lateral friction, and more than 90% of the pile load is supported by lateral friction. The curve of pile–soil stress ratio is hump-shaped, the stress ratio of pile to adjacent pile center soil is 6.08–6.65, and the stress ratio of pile to diagonal pile center soil is 7.5–9.45. Q–S curve of the single pile is characterized as a sharp decline, the characteristic value of the bearing capacity can be obtained by the equation of rigid pile, and the reduction coefficient of the pile strength is 0.25. Q–S curve of the composite foundation performs a slow downward tendency, the characteristic value of the bearing capacity can be obtained by the equation of compacted cement–soil piles, it is suggested that the correction coefficient of the vertical compressive bearing capacity is 1.0, and the bearing capacity correction coefficient of soil between piles is 1.05–1.15.

Keywords Composite Foundation · Cement Stabilized Gravel Pile · Loading tests · Negative friction resistance · Bearing Capacity Characteristics

✉ Xuansheng Cheng
  chengxslut@sina.com

  Fei Gao
  549311069@qq.com

  Yanxu Zhao
  zhaoyx822@sina.com

  Qingfeng Lv
  lvqf@lzu.edu.cn

  Xiangjun Chen
  37198437@qq.com

1   Western Engineering Research Center of Disaster Mitigation
    in Civil Engineering of Ministry of Education, Lanzhou
    University of Technology, Lanzhou 730050, Gansu, China

2   China Railway 21st Bureau Group Co. LTD,
    Lanzhou 730070, Gansu, China

3   Key Laboratory of Mechanics on Western Disaster
    and Environment with the Ministry of Education, Lanzhou
   University, Lanzhou 730000, Gansu, China

1 Introduction

The track structure of a high-speed railway has high precision, when the subgrade is the carrier of the track structure, it must have sufficient strength, stiffness and deformation resistance [1, 2]. According to different geological conditions, the composite foundation of compaction pile, CFG (Cement-fly ash-graved) pile, DDC (Downhole dynamic compaction) pile, long–short pile and pile-plate structure can meet the design requirements of the high-speed railway [3–10]. However, the long-term loading of a high-speed railway subgrade will cause secondary disasters, such as over-limit settlement, arch and lateral slip under extreme weather conditions. The traditional foundation reinforcement method will be limited by the railway electrification network and cannot be implemented. Zhao et al. [11] developed a walking hydraulic rotary pile drilling machine and rammer machine (Fig. 1), which can realize the rapid construction of pile foundation in a limited

Fig. 1 Pile drilling machine and rammer machine

height and space. It is used in compacted cement stabilized gravel piles to control the subgrade settlement of a high-speed railway station, which achieved good results.

Compacted cement stabilized gravel pile is developed based on compacted cement–soil column (flexible pile) and CFG pile (rigid pile), the material of the pile is cement stabilized gravel, which belongs to semi-rigid pile composite foundation, and is mainly used to strengthen soft soil foundations such as loess and clay with saturation less than 65%. The principle of foundation reinforcement is to drill holes with a walking hydraulic rotary pile drilling machine, tamp the cement stabilized gravel with a rammer machine, and compact the soil layer between the piles under the lateral squeezing force generated by tamping to form a composite foundation composed of cement stabilized gravel piles and soil between the piles, it has the advantages of high short-term strength of the pile, simple and fast construction, short construction cycle, small environmental pollution, saving materials and investment. The process flow is shown in Fig. 2. The main construction steps include preparation of drilling rig, drilling hole, removing drilling machine, preparation of rammer machine and ramming material in the hole. Through the implementation of these steps, the composite foundation composed of cement stabilized gravel pile and soil between piles is finally formed.
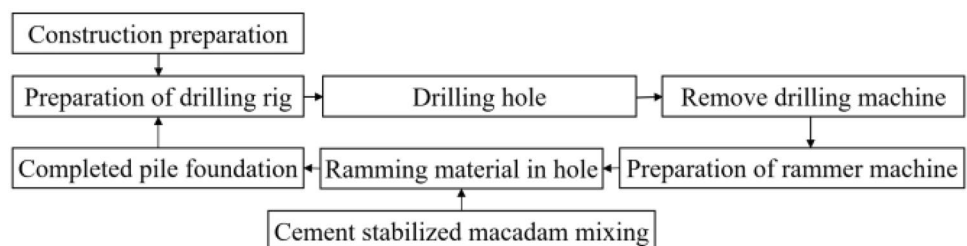
At present, the theoretical research on compacted cement stabilized gravel pile composite foundation lags behind the engineering practice, the existing research mainly focuses on the design parameters [12, 13], construction technology [14–16], quality inspection [17] and reinforcement effect [18, 19] of cement gravel pile composite foundation, and has formed a consensus on the effectiveness of cement gravel pile in treating subgrade diseases. However, there is no in-depth research on the working mechanism of cement gravel pile composite foundation, especially the research on compacted cement stabilized gravel pile is almost blank. Therefore, it is necessary to conduct in-depth research on the bearing characteristics of compacted cement stabilized gravel pile composite foundation, improve the theory of this kind of composite foundation, and better guide the engineering practice.

In this paper, combined with the subgrade disease treatment project of a high-speed railway station, a representative site was selected, and the field load test was designed, Q–S (load–settlement) curves, the axial force of a single pile and the state of lateral friction of the composite foundation with compacted cement stabilized gravel pile under graded load were analyzed. The numerical calculation method was used to analyze the pile–soil stress distribution characteristics, the axial force of the pile and the state of lateral friction of the composite foundation with group piles. The Q–S curve was compared and analyzed, and the bearing characteristics of the composite foundation with compacted cement stabilized gravel pile were discussed, the calculation method of the bearing capacity eigenvalue was suggested, which provides a scientific basis for the design and construction of the composite foundation with compacted cement stabilized gravel pile for the wider promotion and application.

2 Field Test

2.1 Introduction of the Test Site

A high-speed railway station is located in Qilihe district, Lanzhou City, Gansu Province, it is a large passenger transport hub built using the old railway station, including 13 platforms and 28 tracks, the station was constructed in 2009 and it was available to use in July 2017. While subgrade

Fig. 2 Technological process of compacted cement stabilized gravel pile

settlements occurred in the station in a few months, which observably affected the safe operation of the trains. The Compacted Cement Stabilized Gravel Piles project was applied to reinforce the subgrade of the settlement section by the railway engineering department.

The site test is located in the high-speed railway station, and the site geological conditions are consistent with the geological conditions of the settlement subgrade section. The site belongs to the second terrace of the Yellow River with an average elevation of 1537 m. The soil layer properties in exploration depth are described as follows, Artificial filling ($Q_4^{m/3}$), mainly composed of sandy loess, with a depth of 0–4 m, slightly wet–wet, slightly dense, grade II ordinary soil. Sandy loess ($Q_4^{m/3}$), mainly silt, depth 4–15 m, slightly wet–wet, slightly dense, grade II ordinary soil, with grade III self-weight collapsibility. Sandy loess ($Q_4^{m/3}$), mainly silt, gravel sand, depth of 15–30 m, slightly wet–wet, dense, grade II ordinary soil. Coarse round granular soil ($Q_4^{m/6}$), mainly composed of sandstone and granite, sand filling, depth of 30–40 m, wet, dense–dense, grade III hard soil. There is no surface water and groundwater in the exploration area, and the basic properties of each soil layer are shown in Fig. 3.

The test piles are arranged in a square shape, and holes are formed by walking an all-directional rotary hydraulic drilling machine. The pile diameter is 450 mm, the pile length is 10,000 mm, and the pile spacing is 1000 mm × 1000 mm. The pile material is cement stabilized macadam mixture that according to the dense skeleton structure design [20, 21]. The compressive strength is 5.5 MPa, the cementitious material is the cement of type 42.5 ordinary portland cement in 5%, the gravel particle size is 0.075–26.5 mm, the maximum dry density is 2.4 g/cm^3, the layered backfill thickness is 300 mm, the conical rod hammer is tamped, and the packing compaction coefficient greater than 0.95.

2.2 Testing Device and Parameters

2.2.1 Experimental Setup

The field load test is designed according to the slow maintenance load method, the testing device and field load equipment are shown in Fig. 4. The data collection is JD-9A chord sensor measuring instrument and displacement sensor, the bearing platform is a C50 (Its standard cube compressive strength is 50 MPa) reinforced concrete structure. The concrete counterweight, safety pier and benchmark pier are C30 (Its standard cube compressive strength is 30 MPa) concrete precast blocks. The main beam is Chinese standard 45A I-steel, the secondary beam is Chinese standard 28a I-steel, the reference beam is Chinese standard 10 I-steel, and the thickness of sand cushion is 15 cm. A 10 cm gap shall be reserved between the safety buttress and the secondary beam, which shall be adjusted by the base plate. The base plate shall be increased or decreased according to the loading process, and a 3 cm gap shall be maintained throughout the loading process.

2.2.2 Testing Procedures

There are nine steps in the field experiments: (1) confirm the maximum loading, graded loads and structural dimensions of bearing platforms for single pile and composite foundation load tests. (2) Construct the test pile and install the stress sensor in the pile. (3) Clean the top of the test pile and put a sand cushion in thickness of 15 cm, which ensures the pile top and the around soil at the same altitude. (4) The bearing platform model is installed on the surface of the sand cushion, and the concrete of bearing platform is poured. (5) The main beam, secondary beam, benchmark pier and safety pier are installed after 28 days of concrete completion. (6) Four displacement sensors are installed in the four corners of the bearing platform, and two reference beams and data acquisition systems are installed on both sides. (7) The preloading method is used to calibrate the nuclear test system, and the pre-stressed loading is 4% of the maximum value. (8) According to the slow maintenance loading method, each load lasts for 2 h, recording the reading data every 30 min. The next level of loading would be applied until the settlement is less than 0.1 mm in 1 h, and then start the unloading procedure. (9) Data processing. The testing data are the average value of the four displacement sensors, and the Q–S curves are confirmed.
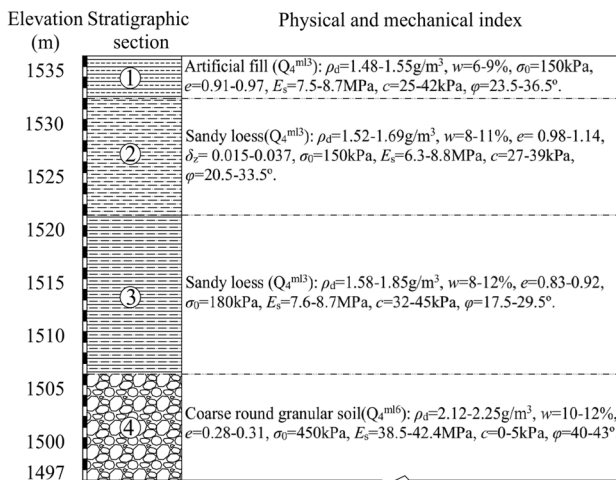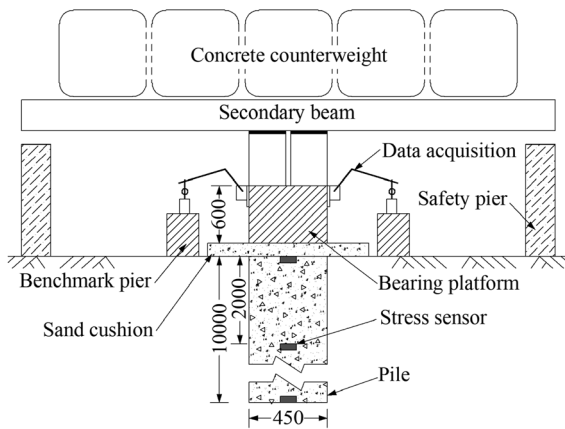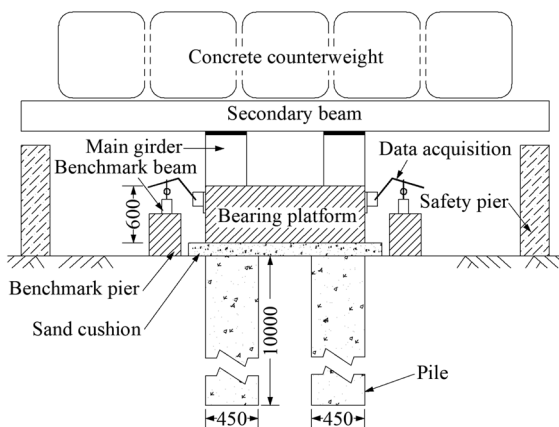
Elevation Stratigraphic   Physical and mechanical index
(m)   section

1535 ① Artificial fill (Q_4^{ml3}): ρ_d=1.48-1.55g/m^3, w=6-9%, σ_0=150kPa, e=0.91-0.97, E_s=7.5-8.7MPa, c=25-42kPa, φ=23.5-36.5°.

1530 ② Sandy loess(Q_4^{ml3}): ρ_d=1.52-1.69g/m^3, w=8-11%, e= 0.98-1.14, δ_z= 0.015-0.037, σ_0=150kPa, E_s=6.3-8.8MPa, c=27-39kPa, φ=20.5-33.5°.

1525

1520

1515 ③ Sandy loess (Q_4^{ml3}): ρ_d=1.58-1.85g/m^3, w=8-12%, e=0.83-0.92, σ_0=180kPa, E_s=7.6-8.7MPa, c=32-45kPa, φ=17.5-29.5°.

1510

1505 ④ Coarse round granular soil(Q_4^{ml6}): ρ_d=2.12-2.25g/m^3, w=10-12%, e=0.28-0.31, σ_0=450kPa, E_s=38.5-42.4MPa, c=0-5kPa, φ=40-43°.

1500

1497

Fig. 3 Physical and mechanical parameters of soil layer

(a)

(b)

Fig.4 Test schematic and field test (unit: mm): **a** single pile test; **b** composite foundation test

2.2.3 Loading test of single pile

To investigate the Q–S curve features of the single pile and the mechanical state of the pile, three piles were selected to perform the loading tests of the single pile, which were numbered as A_1, A_2 and A_3, as shown in Fig. 4. The stress sensors were arranged from top to bottom at the center of the pile according to the spacing of 2000 mm, the axial force and lateral friction resistance of the pile were obtained. The bearing platform is circular, which is a diameter of a section of 450 mm, a thickness of 600 mm, an area of 0.159 m², and a maximum loading load of $2R_a$ (characteristic value of vertical Bearing Capacity of the single pile). Referred to the relevant requirements of the rigid pile in the Chinese *Technical Code for Ground Treatment of Building* [22] and *Technical Code for Ground Treatment of Railway Engineering* [23], the value of R_a is estimated by Eq. (1).

$$R_a \leq \eta f_{cu} A_p, \tag{1}$$

where R_a is the characteristic value of vertical bearing capacity of a single pile (kN). A_p is the pile cross-sectional area (m²), and the value is 0.159. f_{cu} for cement stabilized gravel mixture compressive strength (MPa) and the value is 5.5. η is the pile strength reduction factor and the value is 0.33.

It can be obtained by calculating that R_a is 285 kN, and the maximum loading stress is 570 kN. The loading process is divided into 8 loading stages and 4 unloading stages. The first loading stage is 80 kN, and it is loaded step by step with an incremental loading of 70 kN until 570 kN. The unloading stages are conducted step by step with a decreasing loading of 140 kN, and the last stage is completely unloaded.

2.2.4 Loading Test of the Composite Foundation

Three points are selected to perform the composite foundation loading tests, which are numbered D_1, D_2 and D_3. The load–settlement relationship of the composite foundation is analyzed, and the testing device and field loading test are shown in Fig. 4. The length, width, and height of the loading platform are 2000 mm, 1800 mm and 600 mm respectively, and the area is 3.6 m^2. The maximum loading stress is 2 f_{spk}, and the value of f_{spk} is estimated by Eq. (2), which is referred to the relevant requirements of compacted cement–soil column composite foundation in Chinese *Technical Code for Ground Treatment of Building* [22] and *Technical Code for Ground Treatment of Railway Engineering* [23].

$$f_{spk} = \lambda m \frac{R_a}{A_p} + \beta (1 - m) f_{sk}, \tag{2}$$

where f_{spk} is the characteristic value (kPa) of composite foundation bearing capacity. m is the area replacement rate, which is taken as 0.159. $\lambda = 1$, and it is the correction coefficient of vertical compressive Bearing Capacity of pile. $\beta = 0.9$, which is the correction coefficient of soil Bearing Capacity between piles. $f_{sk} = 180$ kPa, which is the characteristic value of the bearing capacity of soil between piles after treatment.

Based on the calculation, if the $f_{spk} = 420$, and the maximum load is 3000 kN, the stress loading process is divided into 10 loading stages and 5 unloading stages. The first stage load is 300 kN, and it is loaded step by step with 300 kN until it is up to 3000 kN. The unloading stage is completed with 600 kN per stage until the last stage.

2.3 Testing Results and Analysis

2.3.1 The Characteristics of Q–S Curves

The *Q–S* curves of single pile and composite foundation loading tests are drawn in Fig. 5. The *Q–S* curves of A_1, A_2 and A_3 piles in single pile load tests are shown in Fig. 5a, and the *Q–S* curves of D_1, D_2 and D_3 testing points in composite foundation load tests are shown in Fig. 5b.

It can be seen from Fig. 5a that the *Q–S* curve of single pile is a steep drop type, and the ultimate loading is 430 kN. There are two obvious linear deformation sections in the curve: Stage I (0–430 kN), the settlement increased slowly, and the settlement data of A_1, A_2 and A_3 test piles are 5.41 mm, 4.28 mm and 8.37 mm under 430 kN loading condition. In stage II (430–570 kN), the settlement increased rapidly, and the settlement values of A_1, A_2 and A_3 test piles are 26.6 mm, 25.73 mm and 29.6 mm under 570 kN loading condition. Figure 5b shows that the maximum loading in the composite foundation load test is 3000 kN, and the *Q–S* curves show slow deformation without obvious proportion limit and ultimate loading section.

2.3.2 Axial Force and Lateral Friction Resistance of Single Pile

During the single pile loading tests, the compressive stress measured by pile sensor is converted to axial force. The lateral friction resistance is calculated by axial force difference between adjacent sections divided by the lateral surface area of pile. The distribution diagram of pile axial force and lateral friction resistance of single piles are drawn in Fig. 6.

The axial force and lateral friction resistance of the pile increase with the increasing loading stress, and they decrease
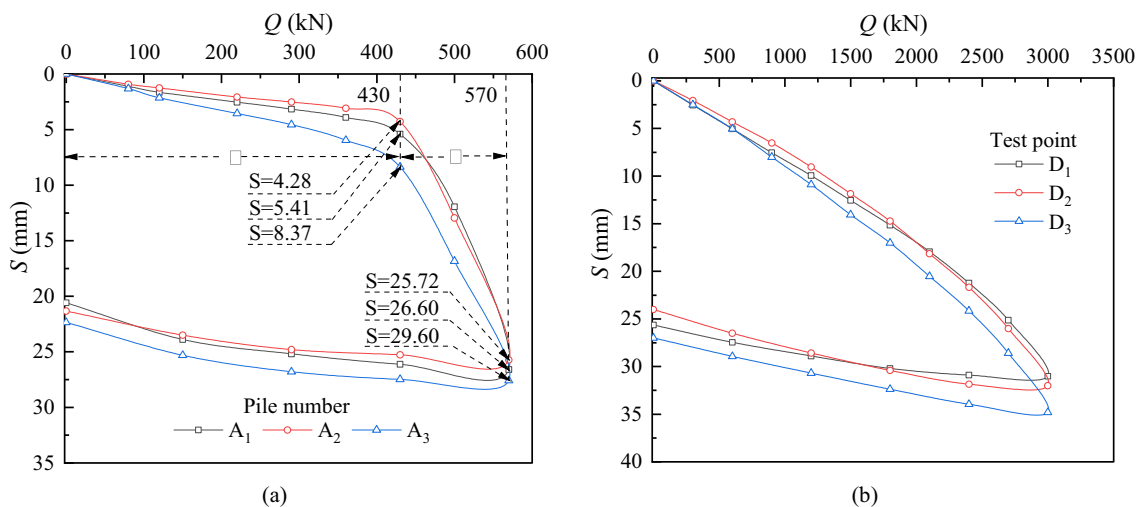

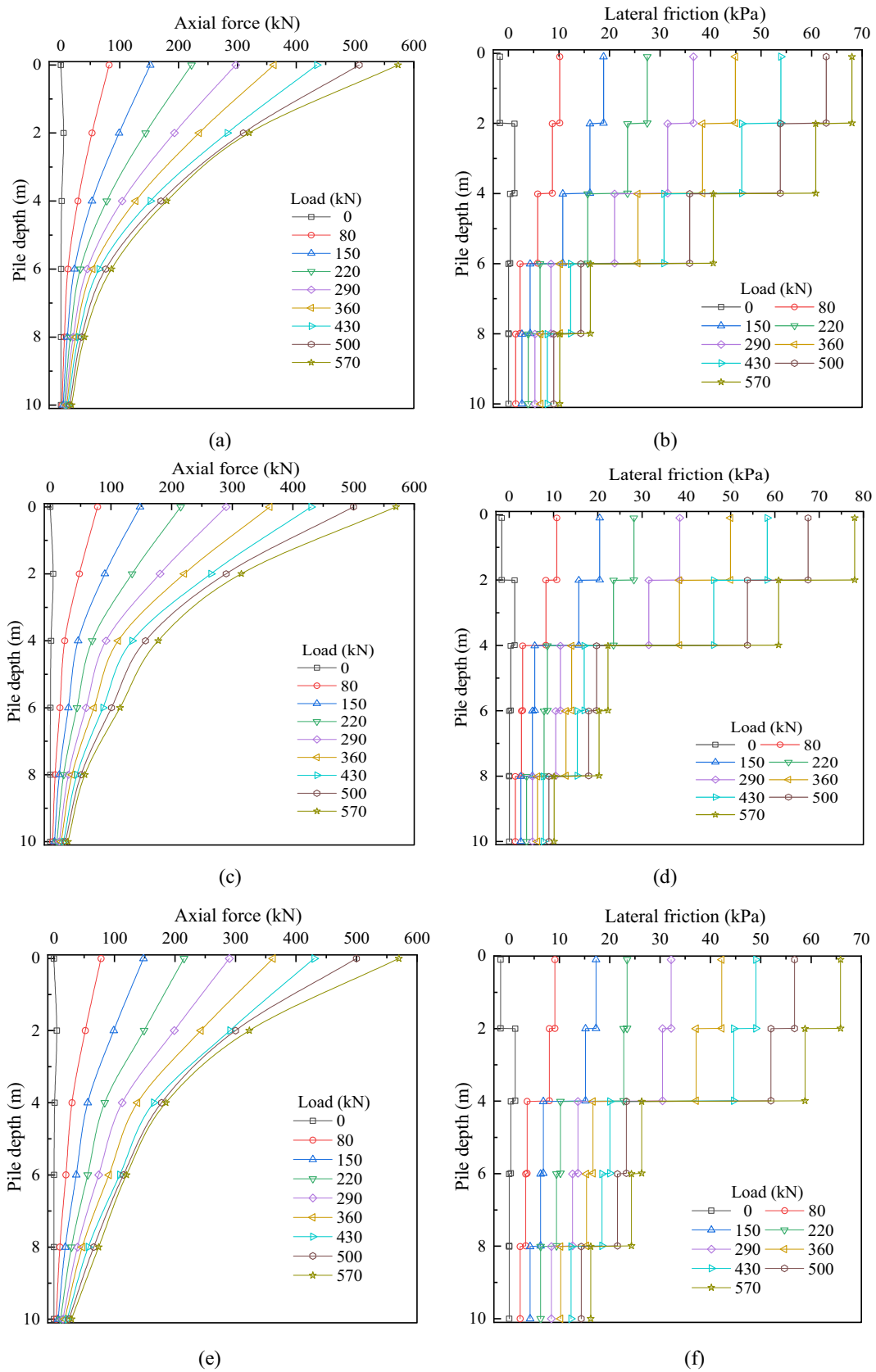**Fig. 5** The *Q–S* curves of load test: **a** single pile test; **b** composite foundation test

Fig.6 Axial force and lateral friction of single pile: **a**, **b** A_1 pile; **c**, **d** A_2 pile; **e**, **f** A_3 pile

with the depth increasing of pile. As the loading stress increases from 0 to 430 kN, the axial force of pile increases linearly. While the loading stress increases from 430 to 570 kN, the axial force curve of pile gradually converges. The pile axial force and lateral friction show more attenuation in depth of 0–4 m, and they perform less attenuation in range of 4–10 m. The maximum axial force and lateral friction of the 0–4 m section are 572 kN and 77.5 kPa respectively, and the maximum axial force and lateral friction of the 4–10 m section are 206 kN and 39 kPa as well.

The distribution of axial force and lateral friction resistance of the single pile shows that the lateral friction resistance of the upper part of pile is exerted before the lower part of the pile. As the load is small, the loading is mainly bore by the lateral friction resistance of the upper soil mass, and with the increase of the loading, the lateral resistance of the lower soil layer gradually exerts. The lateral friction resistance bears about 90% of the loading, while the end resistance plays a negligible role.

3 Numerical Simulation of Composite Foundation

3.1 Numerical Model

Plaxis3d was used to simulate the field loading tests. The model size is shown in Fig. 7a. The bottom boundary of the soil is full constraint, the surrounding boundary is horizontal constraint, and the top is free boundary. An embedded unit is applied for compacted cement stabilized gravel pile [24], the diameter is 450 mm and the pile unit weight is 24 kN/m^2, the constitutive model is Elastic–Plastic, the elastic modulus is 15,000 MPa, the yield stress is 5.5 MPa, the strength reduction coefficient of pile and soil contact interface R_{inten} is 0.88. The lateral friction is related to the soil layer, the Hardening-Soil model is used for artificial filling and sandy loess, and the Mohr–Coulomb model is used for coarse-grained soil and sand cushion, the Linear Elasticity model is used for the bearing platform. There are 10 loading steps, which are consistent with the field testing procedures. The physical and mechanical parameters of the artificial embankment and sandy loess in the model are the test values after foundation reinforcement. The parameters of sandy loess, coarse round granular soil, sand cushion and bearing platform are selected from Fig. 3 [25, 26]. The detailed data are shown in Table 1.

3.2 Analysis of Results

3.2.1 Q–S Curves of Composite Foundation

Based on the numerical simulation results and field test data, Q–S curves of the composite foundation are plotted (Fig. 8), and the reliability of numerical simulation parameters is analyzed.
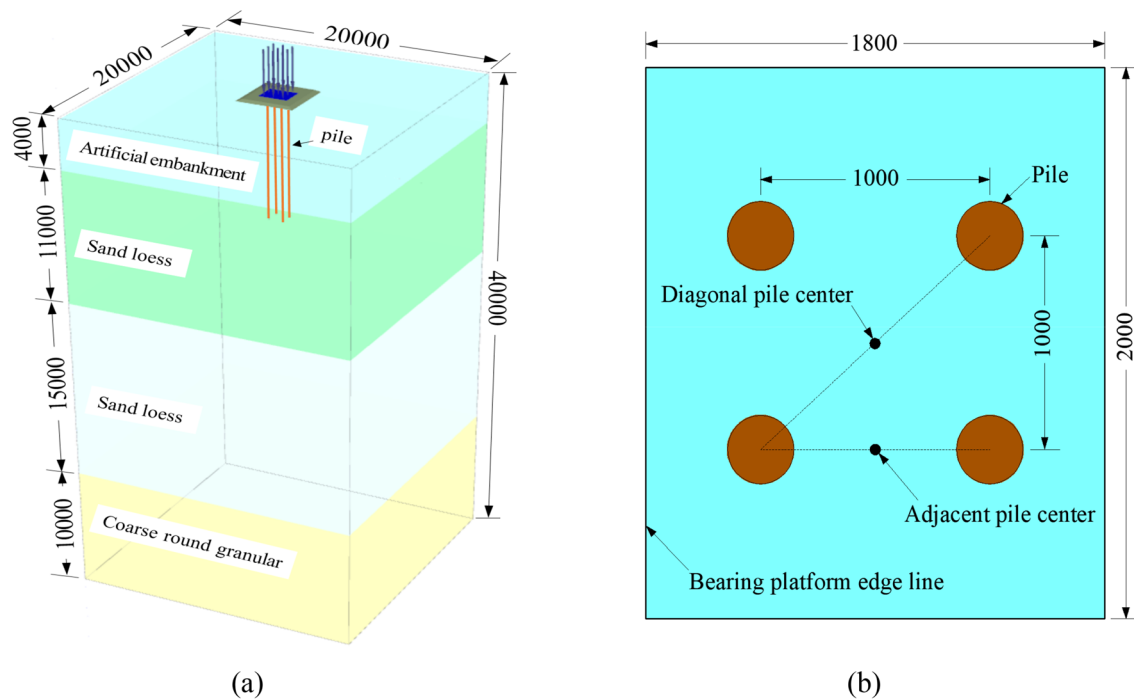

(a)

(b)

Fig. 7 Finite element model (unit: mm): **a** overall model; **b** local schematic of pile foundation

Table 1 Model parameters

Stratum and material	Constitutive model	E_{50}^{ref} (MPa)	$E_{\text{oed}}^{\text{ref}}$ (MPa)	$E_{\text{ur}}^{\text{ref}}$ (MPa)	E (MPa)	μ	φ (°)	c (kPa)	γ (kN/m³)
Artificial embankment	Hardening-Soil	25	25	75	/	0.35	30	45	17.5
Sand loess	Hardening-Soil	26	26	78	/	0.35	28	47	18
Sand loess	Hardening-Soil	28	28	84	/	0.35	26	49	18.5
Coarse round granular soil	Mohr–Coulomb	/	/	/	120	0.28	15	120	20
Sand cushion	Mohr–Coulomb	/	/	/	200	0.33	5	35	22
Bearing platform	Linear elasticity	/	/	/	2.7E+7	0.2	/	/	24

Fig. 8 *Q–S* curves of composite foundation

models are reasonable, and numerical simulation results are dependable to present the bearing capacity characteristics of composite foundation. Based on the above analysis results, the settlements of D_1, D_2, D_3 and numerical results under loading of 1500 kN are 12.55 mm, 11.85 mm, 14.05 mm and 13.01 mm respectively, and they are 31.02 mm, 32.03 mm, 34.82 mm and 32.88 mm under 3000 kN, respectively.

3.2.2 Mechanical Characteristics of Pile in Composite Foundation

Figure 9 shows the distribution curves of the axial force and lateral friction resistance of the pile with the load in the numerical simulation of the composite foundation.

The axial force of pile first increases and then decreases with the pile depth, the maximum and minimum values of axial force are 480 kN and 25 kN. The maximum value is at the pile depth of 2 m, and the minimum value is at the bottom of the pile, which shows that axial force is mainly sustained by the lateral friction of pile, while the end resistance acts a negligible role. The axial force curves of the pile show three stages along the depth of pile as marked in Fig. 9a. The increasing state of the I section curve indicates the pile bears negative friction resistance. In the slow
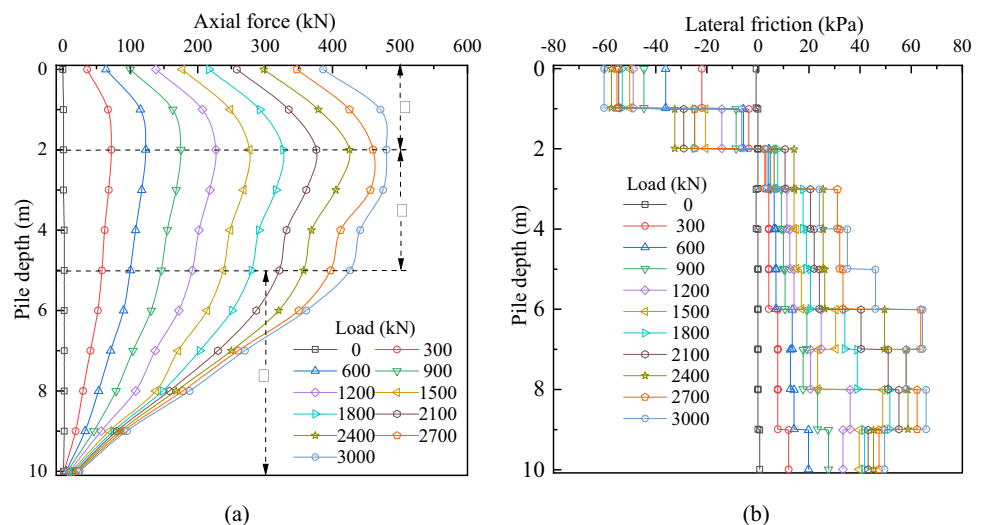
It can be seen from Fig. 8 that *Q–S* curves of numerical simulation and field test are slow drop shape and have a high degree of agreement, indicating that the material parameters, boundary conditions and contact properties in numerical

Fig. 9 Axial force and lateral friction distribution of composite foundation pile: **a** axial force; **b** lateral friction

(a)   (b)

decreasing section of the II section curve, the lateral friction resistance is relatively small. While the steep drop state of the III section curve shows that lateral friction resistance is relatively large. Similar characteristics also can be found in the axial force curves of 2700 kN and 3000 kN conditions, which show that after the load exceeds 2700 kN the lateral friction of the pile gradually tends to be stable. The compression deformation of pile end soil layer and the settlement of pile would gradually increase, which is proved in the Q–S curve of Fig. 8.

Figure 9b shows that negative friction appears in the range of pile depth 0–2 m. The neutral point occurs at the depth of 2 m, which means that the compression deformation of the soil layer at the end of pile is larger than that of the pile, resulting in negative friction of pile. With the increase of loading, the negative friction resistance decreases gradually, while the lateral friction resistance gradually increases in the range of 2–10 m pile depth. The maximum and minimum values of lateral friction resistance are 65 kPa and − 60.5 kPa, the maximum value is in the range of pile depth 8–9 m, and the minimum value is in the range of pile depth 0–1 m. The lateral friction resistance develops gradually from bottom to top during the loading process, and it tends to be stable at around 65 kPa.

The comparative analyses of Figs. 6 and 9 prove that the distribution of axial force and lateral friction resistance of the pile is different. In the single pile load tests, the soil between the piles does not bear the loading, the axial force and lateral friction resistance recede from top to bottom, and the friction resistance is exerted before the lower part at the upper section of pile. In loading tests of the composite foundation of the pile group, the pile in the depth range of 0–2 m appears negative friction resistance, the neutral point is located near the depth of 2 m (1/5 pile length), and the maximum axial force moves down to the depth of 2 m (1/5 pile length), the minimum value occurs at the bottom of the pile. This can be attributed to the soil between the piles bearing the loading, and the deformation of the soil at the end of pile being larger than that of the pile. It results in negative frictional resistance on the upper part of the pile, the friction resistance sustains before the upper part of the pile. In general, lateral friction resistance plays a leading role in both single pile and group pile composite foundation, which bears more than 90% of the loading, and the end resistance presents a lower action.

3.2.3 Distribution Characteristics of Soil Stress Between Piles

According to the numerical simulation results, the monitoring points are shown in Fig. 7b. The pile top stress (σ_p), the adjacent pile center soil stress (σ_a) and the diagonal pile center soil stress (σ_d) are obtained. The pile–soil stress ratio
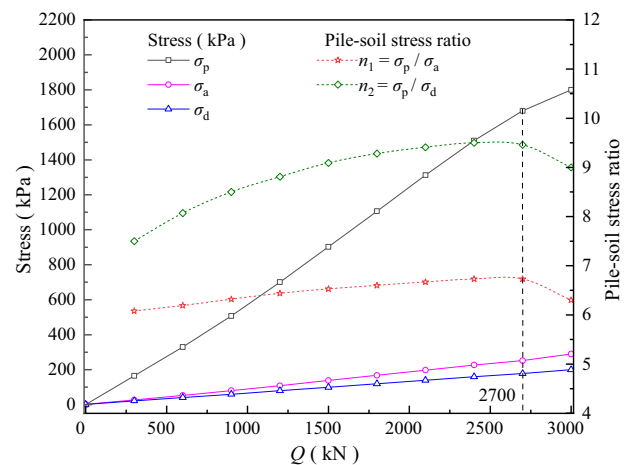

Fig. 10 Pile–soil stress and pile–soil stress ratio

(n_1, n_2) is used to characterize the load sharing features between pile and soil where $n_1 = \sigma_p/\sigma_a$, $n_2 = \sigma_p/\sigma_d$. The distribution curves of soil stress and pile–soil stress ratio between pile top and pile are shown in Fig. 10 under loading conditions.

As can be seen from Fig. 10, when $Q < 2700$ kN, σ_p, σ_a, σ_d and n_1, n_2 are increasing, and the increasing range of σ_p is much higher than that of σ_a and σ_d. The distribution range of n_2 is between 6.03 and 6.65, indicating that the load borne by piles is higher than that borne by the soil between piles. When $Q > 2700$ kN, σ_p increases slowly, increases greatly in σ_a and σ_d, n_1 and n_2 begin to attenuate. When $Q = 2700$ kN, n_1 and n_2 reach the peak value which is 6.65 and 9.45, respectively. It means that the pile begins to fail, the load is borne by soil between piles increasing, n_1 and n_2 begin to decrease when $Q = 2700$ kN. In other words, the ultimate bearing capacity of composite foundation is 2700kN.

3.2.4 Deformation Characteristics of Composite Foundation

Figure 11 shows the vertical displacement and strain distribution of composite foundation under the loading of 2100 kN and 2700 kN conditions.

It can be seen from Fig. 11 that with the increase of loading, the settlement and the strain of soil between piles are larger than that of piles. The settlement and strain of soil around piles are increasing, and the range is also expanding. The positive strain of the surface on both sides of the bearing platform is gradually increasing, indicating that the foundation under the bearing platform is settling and the surface on both sides of the bearing platform is uplifting. The negative friction on the upper section of the pile is caused by the difference between pile and soil settlement.
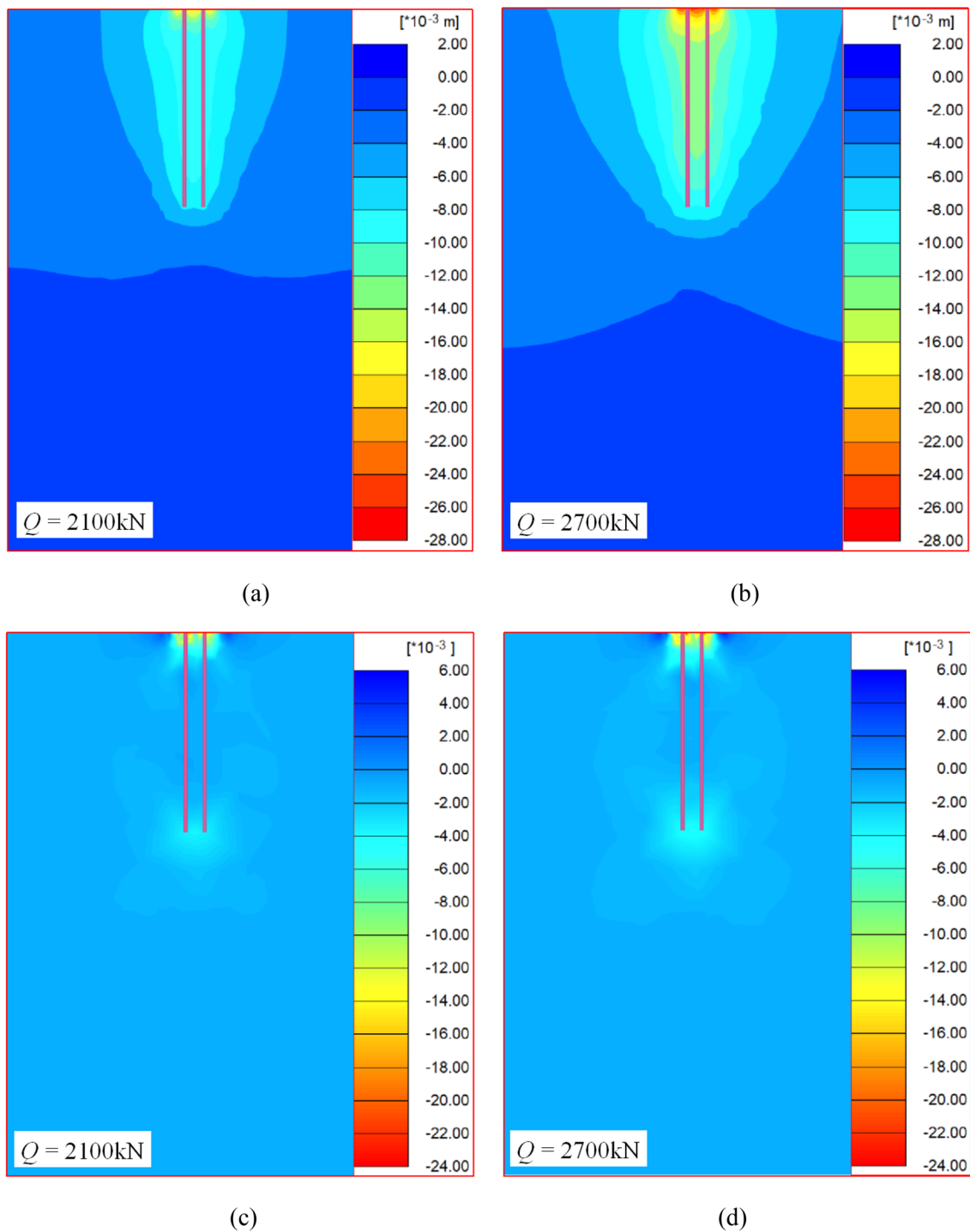
Fig. 11 Deformation characteristics of composite foundation: **a**, **b** vertical displacement; **c**, **d** vertical strain

4 Confirmation of Bearing Capacity

4.1 Characteristic Value of Bearing Capacity

$Q–S$ curve of single pile load test is performed as steep drop type as shown in Fig. 5a. According to the Chinese *Technical Code for Ground Treatment of Building* [22] and the *Technical Code for Ground Treatment of Railway Engineering* [23], the ultimate bearing capacity is 430 kN. As the safety factor is 2.0, the characteristic value of bearing capacity is 215 kN.

From Figs. 5b and 8, it can be seen that Q–S curve of the composite foundation load test is a gentle and smooth curve. According to the suggestion of [22, 23], the $Q = 1500$ kN (417 kPa) can be taken as the characteristic value of composite foundation bearing capacity, but this method is greatly affected by the maximum loading. It can be seen from Fig. 10 that when the $Q = 2700$ kN, the pile has nonlinear deformation. It can be concluded that the ultimate bearing capacity of composite foundation is 2700 kN (750 kPa). As the safety factor is 2.0, the characteristic value of bearing capacity is 1350 kN (375 kPa). From the above analysis, the characteristic value of single pile bearing capacity can be 215 kN and it should be 375 kPa for composite foundation.

4.2 Modification of Estimation Equation of Bearing Capacity Characteristics

In the loading tests, the characteristic value of single pile bearing capacity is 285 kN which is estimated by Eq. (1), then the η is 0.33. The characteristic value of single pile bearing capacity is 215 kN which is determined by the field test, and the η calculated is 0.25. The characteristic value of bearing capacity of composite foundation estimated by Eq. (2) is 420 kPa, λ is 1.00 and β is 0.90, and the characteristic value of bearing capacity of composite foundation is 375 kPa, which is determined by test and numerical simulation.

Reference to the λ and β values of non-compacted hole-forming composite foundation recommended by JGJ 79 [22] and TB 10106 [23] in Table 2, when λ is 1 then β is 1.06. The β increases under the conditions described in this paper, which is consistent with the compaction phenomenon of soil between piles in actual working conditions. Therefore, η in Eq. (1) is 0.25, and λ in Eq. (2) is 1.00. The β refers to the recommended value of compaction pile composite foundation, which is more reliable in the actual conditions.

Table 2 Suggested values of λ and β in the composite foundation

Types of composite foundation	Parameter	
	λ	B
Compacted cement-soil pile	1.00	0.8–1.00
Compaction pile	1.00	1.05–1.15
Piles trusted-expanded with column-hammer	1.00	1.10–1.20
Rigid pile	1.00	0.65–0.90

5 Conclusion

The field loading tests of compacted cement stabilized gravel pile composite foundation is conducted, and the numerical simulation analysis is performed by a 3D finite element method to investigate the bearing capacity characteristics and deformation features of the pile. The distribution of axial force and lateral friction of pile under stepwise loading, the characteristics of the Q–S curves, and the stress distributions of pile and soil are analyzed. The calculation method of the characteristic value of bearing capacity is discussed, and the following conclusions can be obtained:

(1) In the composite foundation, the lateral friction of the pile is more than 90% of the load, the lateral friction of the lower part plays a role before the upper part, and the end resistance shows negligible action. The upper part of the pile bears the settlement load transmitted by the soil between piles, the lower part of the pile bears the pile top load and the settlement load of the soil between piles, which results in negative friction on the upper part of the pile and large lateral friction on the lower part of the pile. The neutral point is located at 1/5 of the pile length. It is suggested that the strength of the pile materials near the neutral point should be properly increased and the roughness of the pile also should be increased to give full play to the lateral friction in the compacted cement stabilized gravel pile composite foundation.

(2) The Q–S curves of single pile show steep drop features, and there is an obvious inflection point in the curve, the values of ultimate load and bearing capacity characteristic of a single pile are 430 kN and 215 kN, respectively. The Q–S curves of the composite foundation present a slowly decreasing shape, and the load corresponding to the peak value of the stress ratio of pile to soil curve can be taken as the ultimate load. The values of the ultimate bearing capacity and the bearing capacity characteristic are 750 kPa and 375 kPa.

(3) The stress ratio of pile to soil curve presents hump shape features when the thickness of the cushion layer is 15 cm under the rigid foundation. There is an obvious peak stress ratio, the stress ratio between the pile and the adjacent pile center soil is 6.08–6.65, and the stress ratio between the pile and the diagonal pile center soil is 7.5–9.45. The direct load sharing between the pile and the soil can be adjusted by adjusting the thickness of the cushion layer.

(4) The characteristic value of single pile bearing capacity can adopt the calculation equation of rigid pile in the specification, and the strength reduction coefficient of

pile can be taken as 0.25. The characteristic value of composite foundation bearing capacity can adopt the calculation equation of compacted cement–soil column in the specification. The correction factor of vertical compressive bearing capacity of pile can be taken as 1, and the correction factor of soil bearing capacity between piles can be 1.05–1.15.

(5) The bearing characteristics of composite foundations are analyzed when the cushion thickness is 15 cm under the rigid foundation. The bearing characteristics of compacted cement stabilized gravel pile composite foundations under flexible load and different cushion structures will continue to be studied, and a more scientific design theory and practice method will be proposed to promote the development and application of engineering.

Data Availability All data, models, and code generated or used during the study appear in the submitted article.

Declarations

Conflict of interest The authors declare that there are no conflicts of interest regarding the publication of this paper.

References

1. Choi, C. Y., & Jung, J. H. (2018). Study of the long-term behavior characteristics of roadbed on concrete track of high-speed railway. *Journal of the Korea Academia-Industrial cooperation Society, 19*(4), 8–16. https://doi.org/10.5762/KAIS.2018.19.4.8
2. Tan, Q. L., Li, L. J., & Wang, S. L. (2014). Measurement and analysis of high-speed railway subgrade settlement in China: A case study. *Sensors & Transducers, 170*(5), 184–191.
3. Cheng, X. S., Liu, G. N., Gong, L. J., Zhou, X. H., & Shi, B. Z. (2020). Mechanical characteristics+differential settlement of CFG pile and cement-soil compacted pile about composite foundation under train load. *Geomechanics and Engineering, 20*(2), 155.
4. Cheng, X. S., Zhang, W. L., Zha, W. X., Zhou, Y. C., & Gong, L. J. (2020). Mechanical characteristics of pile-net composite foundations in collapsible loess areas. *Jordan Journal of Civil Engineering, 14*(3), 443–449.
5. Gao, C. H., Du, G. Y., Liu, S. Y., Zhang, D. W., Zhang, K., & Zeng, B. (2020). Field study on the treatment of collapsible loess using vibratory probe compaction method. *Engineering Geology, 37*(4), 591–598. https://doi.org/10.1016/j.enggeo.2020.105715
6. Shi, B. Z., Cheng, X. S., Gong, L. J., & Liu, G. N. (2020). Selection design and parameter optimization of composite foundations in collapsible loess areas. *Geotechnical and Geological Engineering, 38*, 3175–3201. https://doi.org/10.1007/s10706-020-01216-6
7. Xiao, D., Jiang, G. L., Liao, D., Hu, Y. F., & Liu, X. F. (2018). Influence of cement-fly ash-gravel pile-supported approach embankment on abutment piles in soft ground. *Journal of Rock Mechanics and Geotechnical Engineering, 10*(5), 977–985. https://doi.org/10.1016/j.jrmge.2018.06.001
8. Xiao, H., Guo, X., & Huang, L. W. (2015). Analysis of the effect of groundwater exploitation on high-speed railway Pile-Slab

9. structure subgrade. *The Open Mechanical Engineering Journal, 9*, 455–459. https://doi.org/10.2174/1874155X01509010455
9. Zhang, D. B., Zhang, Y., Kim, C. W., Meng, Y., Garg, A., Garg, A., & Fang, K. (2018). Effectiveness of CFG pile-slab structure on soft soil for supporting high-speed railway embankment. *Soils and Foundations, 58*(6), 1458–1475. https://doi.org/10.1016/j.sandf.2018.08.007
10. Zhou, S. H., Wang, B. L., & Shan, Y. (2020). Review of research on high-speed railway subgrade settlement in soft soil area. *Railway Engineering Science, 28*(2), 129–145. https://doi.org/10.1007/s40534-020-00214-x
11. Zhao, Y. X., Chen, X. J., Pan, L., & Duan, L. B. (2019). Walking omnidirectional rotary hydraulic pile drilling machine. China, 201922304247.3, 2019-12-20
12. Wu, Y. (2021). Application of dry mix cement gravel pile in roadbed reinforcement. *Journal of Huaibei Vocational and Technical College, 21*(3), 107–111. https://doi.org/10.16279/j.cnki.cn34-1214/z.2022.03.023
13. Zhang, J. B. (2021). Numerical simulation for weak subgrade strengthening cement gravel mixing trenchless pile. *Highway, 66*(4), 18–22.
14. Bi, D. (2013). Gravel pile of dry mixed cement trial research in reinforcing subgrade. *China Engineering Consulting, 12*(1), 58–61. https://doi.org/10.3969/j.issn.1006-9607.2013.12.001
15. Chen, W., & Li, Y. Z. (2014). Analysis on cement gravel pile application in soft foundation treatment construction of expressway. *Transportation Science & Technology, 267*(7), 66–69. https://doi.org/10.3963/j.issn.1671-7570.2014.06.021
16. Wang, S. W., Wang, Z. F., & Liu, H. D. (2009). Testing on dry mixed cement gravel pile in embankment of Xuchang-Luohe Section of Beijing-Zhuhai Expressway. *Rock and Soil Mechanics, 30*(5), 1421–1424. https://doi.org/10.1016/S1874-8651(10)60073-7
17. Yu, J. Y. (2015). Application of cement stabilizing sand-gravel pile with tamp filling in treatment technology of roadbed frost damage. *Water Resources & Hydropower of Northeast, 367*(2), 13–16. https://doi.org/10.3969/j.issn.1002-0624.2015.02.005
18. Tan, B. S., & Deng, C. (2019). Experimental study on road performance of retailing backwall new filling subgrade reinforced with cement-gravel pile. *Journal of Water Resources Water Engineering, 30*(2), 225–230. https://doi.org/10.11705/j.issn.1672-643X.2019.02.35 238.
19. Zhao, E. S. (2021). Experimental study on treatment of secondary diseases of loess foundation with cement graded crushed stone rammed pile. *Lanzhou: Lanzhou Jiaotong University*. https://doi.org/10.27205/d.cnki.gltec.2021.000648
20. Liu, S. T., Liu, S. J., Liu, T. L., Dai, J. G., & Cao, W. D. (2020). Design method for gradation of skeleton-density cement stabilized macadam. *Journal of Huaqiao University (Natural Science), 41*(5), 582–588. https://doi.org/10.11830/ISSN.1000-5013.201912039
21. Zhao, L. J., Jing, W. Z., Hou, J. R., Feng, Z. X., & Xue, S. Q. (2018). Influence of mixing method on performance of compressive strength for cement stabilized macadam mixture. *China Journal of Highway and Transport, 31*(1), 151–158. https://doi.org/10.19721/j.cnki.1001-7372.2018.01.018
22. JGJ 79-2012. (2012). *Technical code for ground treatment of buildings*. Beijing: China Building Industry Press. in Chinese.
23. TB 10106. (2010). Technical code for ground treatment of railway engineering. China Railway Publishing House (i**n Chinese**)
24. Granitzer, A. N., & Tschuchnigg, F. (2021). Practice-oriented validation of embedded beam formulations in geotechnical engineering. *Processes, 10*(9), 1–27. https://doi.org/10.3390/pr9101739
25. Kaya, O., Zhang, Y., Ceylan, H., Kim, S., Yang, S., Taylor, P. C., & Gopalakrishnan, K. (2019). Numerical analysis of longitudinal cracking in widened jointed plain concrete pavement systems.

International Journal of Pavement Research and Technology, 12(3), 277–287. https://doi.org/10.1007/s42947-019-0034-z

26. Wang, L. J., Hu, C. B., & Zeng, Y. X. (2017). Numerical analysis of early-age curing behavior of cement concrete pavement. *Engineering Mechanics, 34*(7), 146–155. https://doi.org/10.6052/j.issn.1000-4750.2016.02.0121

Fei Gao (1983.10-), senior engineer, master of Lanzhou University, doctoral student of Lanzhou University of Technology, mainly studies disaster prevention and mitigation of road and railway engineering.

Xuansheng Cheng (1972.5-), Ph.D., Professor of Lanzhou University of technology, doctoral supervisor, mainly studies civil engineering disaster prevention and mitigation.

Yanxu Zhao (1972.8-), Ph.D., professor, mainly studies the prevention and control of geological disasters in railway engineering, and the construction and management of high-speed railways.

Qingfeng Lv (1971.4 -), Ph.D., Professor of Lanzhou University, mainly studies new subgrade structure.

Xiangjun Chen (1970.10-), bachelor, professor, mainly studies the construction and management of high-speed railway.